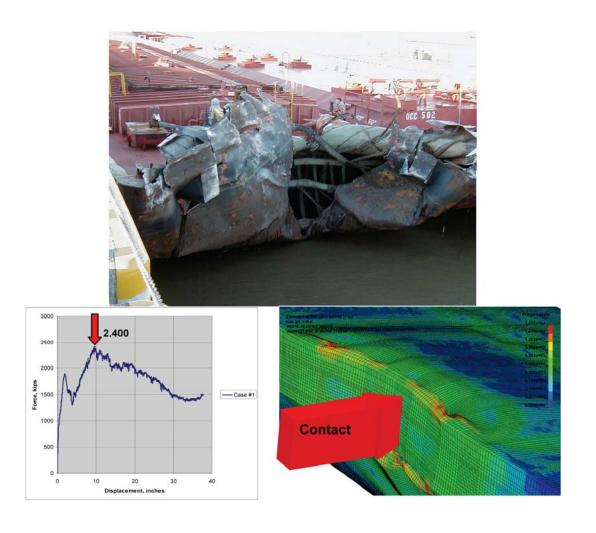


Limiting Impact Force Due to Yielding and Buckling of the Plates and Internal Structural Frame at the Bow of a Barge during Its Head-on Impact with a Bullnose or Cellular Structure

Robert M. Ebeling and Terry W. Warren

August 2009



Approved for public release; distribution is unlimited.

Limiting Impact Force Due to Yielding and Buckling of the Plates and Internal Structural Frame at the Bow of a Barge during Its Head-on Impact with a Bullnose or Cellular Structure

Robert M. Ebeling and Terry W. Warren

Information Technology Laboratory U.S. Army Engineer Research and Development Center 3909 Halls Ferry Road Vicksburg, MS 39180-6199

Final report

Approved for public release; distribution is unlimited.

Prepared for Headquarters, U.S. Army Corps of Engineers

Washington, DC 20314-1000

Under Work Unit J4J37B

Abstract: This report presents a research study conducted to predict the impact forces that occur when a barge train impacts head-on with a circular concrete or concrete-filled structure. These structures are found at the end of lock approach walls as semicircles called bullnoses, as circular cells, and as mooring cells. This research was conducted using finite element analysis. A detailed finite element model of the bow of a jumbo hopper barge was created. LS-DYNA was used to perform impact simulations of the barge bow impacting differing diameters of cell structures and at varying approach velocities. In each case a "capping force" was found caused by the plating and internal structure acting as a "fuseplug" during the crushing of the bow.

Although research projects have been performed focused on corner barge impacts with lock walls, little research has been conducted in the area of forces from head-on collisions between a barge and a bullnose or a cell. A complementary R&D effort has been conducted by Dr. Gary Consolazio and his research associates at the University of Florida. His research has focused on a barge impacting a bridge pier. Comparison with their results has been made when it was appropriate.

DISCLAIMER: The contents of this report are not to be used for advertising, publication, or promotional purposes. Citation of trade names does not constitute an official endorsement or approval of the use of such commercial products. All product names and trademarks cited are the property of their respective owners. The findings of this report are not to be construed as an official Department of the Army position unless so designated by other authorized documents.

DESTROY THIS REPORT WHEN NO LONGER NEEDED. DO NOT RETURN IT TO THE ORIGINATOR.

ERDC/ITL TR-09-3 iii

Contents

Figures and Tables		iv
Pre	eface	vi
Un	it Conversion Factors	vii
1	Introduction	1
	1.1 Background: barge train maximum impact forces	1
	1.2 Yielding and plate buckling analyses	2
	1.3 Nonlinear structural dynamic analyses using LS-DYNA	2
	1.4 Report contents	4
2	Finite Element Mesh and Material Properties	5
	2.1 Introduction	5
	2.2 Finite element mesh	6
	2.3 Material modeling and material properties	11
3	Limiting Impact Force Computations	13
	3.1 Introduction	13
	3.2 Nonlinear impact analyses	14
	3.3 Results	17
	3.4 Comparison with an earlier finite element model	29
	3.5 Comparison with AASHTO specification of impact force as a function of crush	
	depth	
	3.6 Comparison with barges impacted using the 14-MN Statnamic load device	35
4	Summary, Results, and Conclusions	39
	4.1 Summary	39
	4.2 Results	39
	4.3 Conclusions	39
Re	ferences	41

Report Documentation Page

Figures and Tables

Figures

Figure 1.1. Overhead views of the impact area of the bow	3
Figure 1.2. Force versus displacement of the initial contact point of the bow for Case 1, impact with a 20-ft-diameter bullnose at 2 ft/sec.	4
Figure 2.1. Side view of the bow of a raked section, jumbo open-hopper barge	5
Figure 2.2. Mesh of bow-side view of the hull and hopper plates	7
Figure 2.3. Front elliptical corner view of the deck plates, headlog, and elliptical corner of the bow	7
Figure 2.4. View of the bow of the barge at the center-line cut of the bow	8
Figure 2.5. Overhead view of the bow of the barge	8
Figure 2.6. Internal views of the structural trusses at the bow as viewed from one side of the barge looking laterally across the barge	9
Figure 2.7. Another view of the interior showing the truss joining the C-channel of the bow	9
Figure 2.8. Internal structural members with the deck and hull plates removed	10
Figure 2.9. True stress versus true strain for A-36 structural steel	12
Figure 3.1. Diagrams showing the two points of first contact	13
Figure 3.2. The upstream middle wall bullnoses at Smithland Locks and Dam	15
Figure 3.3. Proposed approach wall design for Lock and Dam 22	16
Figure 3.4. Barge train indicating movement in the x-direction only at impact	17
Figure 3.5. Distribution of effective plastic strain (in decimal fraction) at 9.6 in. permanent deformation and force versus displacement plot of the first contact point of the bow for Case 1, usual loading condition at the barge center line and impact with a 20-ft-diameter bullnose structure.	19
Figure 3.6. Distribution of effective plastic strain (in decimal fraction) at 9.6 in. of permanent deformation and erosion of elements in the impact area for Case 1, a usual loading condition impacting a 20-ft-diameter structure	19
Figure 3.7. Distribution of von Mises stress at 9.6 in. permanent deformation and force versus displacement plot of the first contact point of the bow for Case 1, usual loading condition at the barge center line and impact with a 20-ft-diameter bullnose structure	20
Figure 3.8. Distribution of effective plastic strain (in decimal fraction) at 36 in. permanent deformation and force versus displacement plot of the first contact point of the bow for Case 1, usual loading condition at the barge center line and impact with a 20-ft-diameter bullnose structure	21
Figure 3.9. Distribution of effective plastic strain (in decimal fraction) at 36 in. of permanent deformation and erosion of elements in the impact area for Case 1, a usual loading condition impacting a 20-ft-diameter structure.	
Figure 3.10. Distribution of von Mises stress at 36 in. permanent deformation and force versus displacement plot of the first contact point of the bow for Case 1, usual loading condition at the barge center line and impact with a 20-ft-diameter bullnose structure	22
Figure 3.11. Force versus displacement curves for Cases 1 and 2	23

Figure 3.12. Force versus displacement curves for Cases 3 and 4	24
Figure 3.13. Force versus displacement curves for Cases 5 and 6	25
Figure 3.14. Force versus displacement curves for Cases 7 and 8	26
Figure 3.15. Force versus displacement curves for Cases 9 and 10	27
Figure 3.16. Force versus displacement curves for Cases 11 and 12	28
Figure 3.17. Force versus displacement curve for 4-ft-diameter impactor	30
Figure 3.18. Barge bow potential energy for LS-DYNA analysis Case 1	33
Figure 3.19. Force versus displacement curves for LS-DYNA analysis Case 1 and the corresponding AASHTO specification	34
Figure 3.20. Statnamic device and experimental setup during experiment	36
Figure 3.21. Crushing damage of barge headlog	37
Tables	
Table 3.1. Three design load condition categories, frequency of loadings, and typical ranges for non-site-specific impact angles and approach velocities	14
Table 3.2. Parameters that are the basis of the twelve test conditions	17
Table 3.3. Maximum values indicated during head-on barge impacts	29
Table 3.4. Comparison of LS-DYNA and AASHTO specification results for the energy determined from LS-DYNA Case 1 analyses	35
Table 4.1 Summary of maximum impact forces during head-on impacts	40

Preface

Funding to initiate research and software development was provided by Headquarters, U.S. Army Corps of Engineers (HQUSACE), as part of the Infrastructure Technology Research Program. Funding to conclude this research task, including software development, was provided by the Navigation Systems Research Program. The research was performed under Work Unit J4J37B, entitled "Vessel/Barge Impact," for which Dr. Robert M. Ebeling, Computational Science and Engineeing Division (CSED), Information Technology Laboratory (ITL), U.S. Army Engineer Research and Development Center (ERDC), was the principal investigator. The HQUSACE technical monitor was Anjana Chudgar, CECW-CE.

James Clausner, Coastal and Hydraulics Laboratory (CHL), ERDC, was the Navigation Systems Research Program manager, and Dr. John Hite was the Inland Navigation Focus Area leader. Dr. Michael Sharp was Acting Technical Director for Navigation. Angela Premo was the Navigation business line leader, HQUSACE.

The authors thank Dr. Richard Weed, ERDC Computational Structural Mechanics computational technology area on site for the Department of Defense High-Performance Computing Modernization Program (HPCMP) User Productivity Enhancement and Technology Transfer (PET), for his support during the development of the finite element model of the barge and his advice on running LS-DYNA. The authors also thank Robert Alter, ERDC High-Performance Computing (HPC) Department of Defense Shared Resource Center (DSRC) lead (LM), for his assistance with setting up script files and batch jobs on the high-performance computers at ERDC DSRC.

This report was prepared by Dr. Robert M. Ebeling and Terry W. Warren, Sensors, Measurement, and Instrumentation Branch, CSED. Dr. Ebeling was author of the scope of work for this research. The report was prepared under the supervision of Dr. Robert M. Wallace, Chief, CSED, and Dr. Reed Mosher, Director, ITL.

COL Gary E. Johnston was Commander and Executive Director of ERDC. Dr. James R. Houston was Director.

ERDC/ITL TR-09-3 vii

Unit Conversion Factors

Multiply	Ву	To Obtain
feet	0.3048	meters
inches	0.0254	meters
kip-feet	1.3558179	kilonewton-meters
kip-inches	0.1129848	kilonewton-meters
kips (1,000 lbf)	4.448222	kilonewtons
kips (1,000 lbf) per square inch	6,895.3991	kilonewtons per square meter

1 Introduction

1.1 Background: barge train maximum impact forces

Locks are a necessary structural feature found at every dam within the U.S. inland waterways navigation system. This network of rivers is an essential component of the nation's transportation infrastructure system, a system key to national commerce. Locks allow for groups of barges, lashed together to form barge trains, to negotiate the changes in river elevation at the dams. One of the loads applied to the locks of the U.S. inland waterway system is the head-on impact of a barge train with the semicircular portion of bullnose structures or with concrete-filled cell structures. (In this report the term bullnose will be used to refer to either of these two types of structures as the geometry of the contact area is the same for both.) The photograph on the cover of this report shows a badly damaged barge bow after an impact with the bullnose on the upstream lock approach wall at Smithland Lock and Dam on the Ohio River. These loads do not happen frequently as they are generally the result of loss of control of the barge train. However, they do occur, and the potential for occurrence always exists. Consequently this load case is a design consideration for bullnose and cell structures.

This research report discusses the results of a series of nonlinear finite element analyses computing the limiting impact force caused by yielding and buckling of the deck and skin plates and the internal structural frame within the center area of the bow of a jumbo open-hopper barge during a head-on impact with a bullnose or cell structure. The structural concept can be explained as follows. Because of the elastoplastic and limiting strain material characteristics of steel combined with the structural layout of the deck and hull plate, the internal structural plates, and the angle steel of the internal trusses, the multi-degree-of-freedom structure of the barge bow provides a limiting force resistance when significant permanent structural deformation occurs during an impact event. When placed in a severeimpact environment in which the bow begins to crush, the barge bow will act like a structural fuseplug to provide for a limiting impact force applied to the bullnose or cell by the barge train. Thus, there is an upper-bound force that bullnoses and cells will be subjected to during a head-on impact event. This report summarizes the research effort investigating the magnitude of this limiting force. The barge used in this study is a rake

section, jumbo open-hopper barge 200 ft long, 35 ft wide, and 13 ft high¹ at the hopper section region.

1.2 Yielding and plate buckling analyses

In the LS-DYNA nonlinear finite element analyses discussed in this report, the impact areas at the bow of the barge and the approach bullnose (modeled as a nonpenetrating rigid structure) are brought into contact with each other at a constant velocity in the numerical simulation of the crushing of the impact area of the barge bow. Crushing of the bow area continues until 36 in. of penetration of the approach wall into the barge bow is achieved. Figure 1.1a shows an overhead view of the barge bow at initial contact with the bullnose in the numerical analysis using LS-DYNA; Figure 1.1b shows an overhead view of the barge bow after 36 in. of penetration for one of the numerical evaluations. Figure 1.2 shows the corresponding resultant contact force normal to the rigid bullnose, as computed by LS-DYNA during the course of this numerical analysis. The key observation is that the contact force between the rigid nonpenetrating bullnose and the bow increases in magnitude with bullnose penetration into the barge up to a peak force value: the limiting contact force. Continued deformation beyond approximately 10 in. results (for Case 1) in a lower contact force.

Figure 1.2 is an example of typical resultant contact force normal to the rigid (approach) bullnose versus permanent deformation computed at the point of first contact with the barge in the LS-DYNA nonlinear numerical analyses. In this figure, the normal force ranges in value from 0 kip to a maximum force of 2,400 kips at 9.6 in. of permanent normal deformation at the impact point of the bow. All LS-DYNA analyses were continued out to 36 in. of permanent displacement of the bullnose into the bow of the barge.

1.3 Nonlinear structural dynamic analyses using LS-DYNA

LS-DYNA (Livermore Software Technology Corporation 2007) is a general-purpose transient finite element program that is used for analyzing complex structural dynamics problems, such as the crushing of the impact area of the bow of a barge during a head-on impact with a bullnose at the end of a lock wall or with a concrete-filled cell structure. It uses a central difference scheme to solve the equation of motion in time.

¹ A table of factors for converting non-SI units of measure to SI units is found on page vii.

-

Key features used in the analyses discussed in this report are nonlinear dynamics, use of a nonlinear elastic-plastic constitutive model for all A-36 steel plates and angles composing the barge, and use of contact surface formulation for a flexible-body-to-rigid-body contact. Lagrangian shell elements are used to model the barge components.

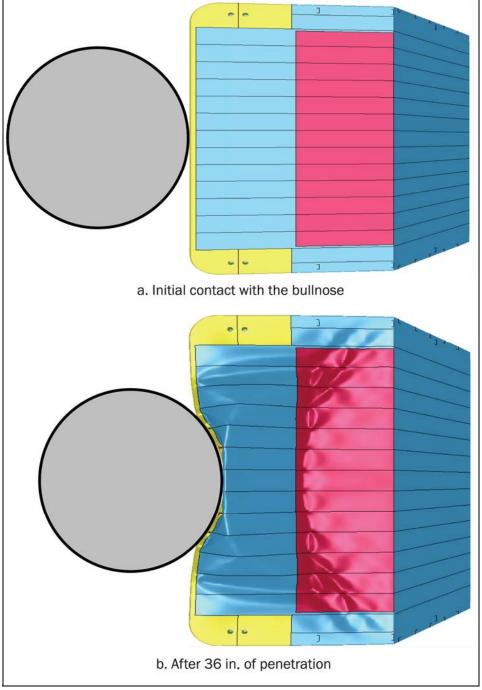


Figure 1.1. Overhead views of the impact area of the bow.

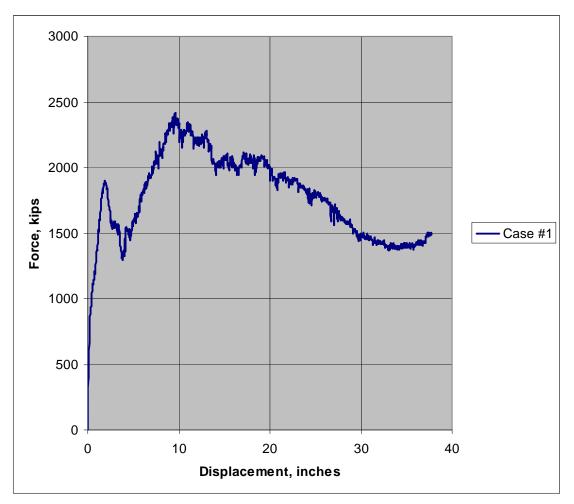


Figure 1.2. Force versus displacement of the initial contact point of the bow for Case 1, impact with a 20-ft-diameter bullnose at 2 ft/sec.

1.4 Report contents

Chapter 2 discusses the finite element mesh for the bow of the jumbo open-hopper barge as well as the assigned material properties. This mesh was assembled using TrueGRID (Rainsberger 2006) and modeled in the nonlinear LS-DYNA analyses. Material properties corresponding to A-36 steel, obtained from tests conducted on plate steel from a barge, are assigned in these numerical analyses.

Chapter 3 reports on the results of the 12 LS-DYNA nonlinear finite element analyses. The diameter of the bullnose structure, the approach velocity, and the location of first contact between the barge and the bullnose are varied among the analyses.

Chapter 4 presents the summary, results, and conclusions.

2 Finite Element Mesh and Material Properties

2.1 Introduction

This chapter discusses the development of the finite element mesh and the material properties assigned to the structural steel composing the barge. The object of the nonlinear finite element analysis using LS-DYNA is to compute the limiting impact force resulting from the yielding and buckling of the plates and internal structural framing of a barge during a head-on impact with a bullnose structure; therefore, only the bow region of the jumbo open-hopper barge needs to be modeled in the numerical analysis (Figure 2.1, raked section).



Figure 2.1. Side view of the bow of a raked section, jumbo open-hopper barge.

The bow is 35 ft wide, 27.7 ft long, and 15.5 ft high. At the intersection of the inclined open-hopper face with the flat hopper base, the barge is 13 ft high.

2.2 Finite element mesh

The mesh generation software TrueGRID was used to construct the finite element mesh of the bow of the jumbo open-hopper barge. Fully integrated LS-DYNA shell elements (*SECTION_SHELL; ELFORM 16) were used in a detailed model (Figure 2.2) of the jumbo open-hopper barge bow structural steel deck, hull, and internal structural plates, as well as the internal angle steel making up the internal structural trusses. 1 The mesh consisted of 357,897 nodes and 353,646 elements. The resulting mesh of the bow of the barge is shown in Figures 2.3–2.5. Also identified by color designation in these figures are the thicknesses of the structural deck, hull, and hopper plates of the bow of the jumbo open-hopper barge. The headlog and elliptical impact corner sections of the bow are shown in yellow in Figures 2.3 and 2.5. The rounded hull plate connecting the front and side hull plates (in blue) is shown in brown in Figures 2.2 and 2.3. Figure 2.4 shows the barge sliced longitudinally along the center line and allows a view of the internal truss system within the bow of the barge as well as the deck and hull plates. Seven internal trusses (six "standard" longitudinal and one outboard longitudinal truss) are contained within this half-bow structural section model. The trusses are made out of A-36 steel angles. Figures 2.6 and 2.7 provide an internal view of the actual structural trusses joining to the vertical C-channel and the pair of horizontal C-channels that provide rigidity of the headlog at the bow of the barge. These figures also show the corresponding finite element meshes of these areas. Figure 2.8 shows the internal structural members with the deck and hull plates removed. Figure 2.8a shows the members as viewed from above looking down at the barge. The starboard side of the barge is on the left. Figure 2.8b shows the internal structural members as viewed from the port side looking to starboard.

¹ LS-DYNA reduced integrated shell elements (*SECTION_SHELL; ELFORM = 2; NUMBER OF INTEGRATION POINTS = 3) with hourglass control (*HOURGLASS; Hourglass Control Type=4, Flanagan-Belytschko stiffness form) were tried to save on execution time in an earlier study (Ebeling and Warren 2008). Reduced integration resulted in execution times nearly one-third that for the fully integrated

elements. However, the results obtained varied significantly if the number of processors used to run a problem was varied. Therefore, the fully integrated shell element model is used. The results obtained from runs with varying numbers of processors are observed to be more consistent.

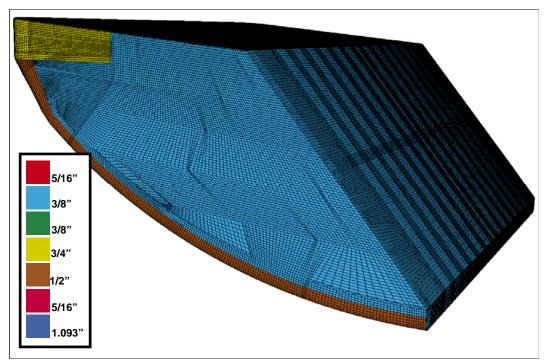


Figure 2.2. Mesh of bow-side view of the hull and hopper plates.

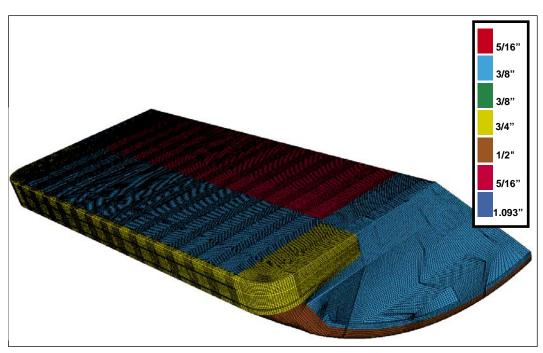


Figure 2.3. Front elliptical corner view of the deck plates, headlog, and elliptical corner of the bow.

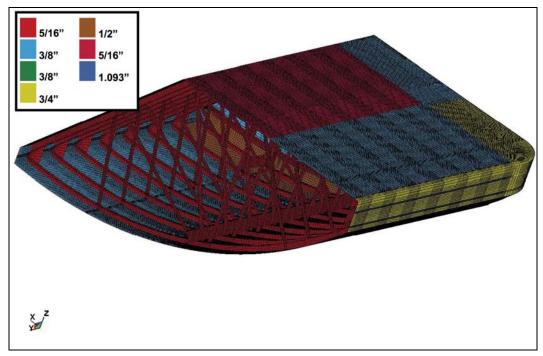


Figure 2.4. View of the bow of the barge at the center-line cut of the bow.



Figure 2.5. Overhead view of the bow of the barge.

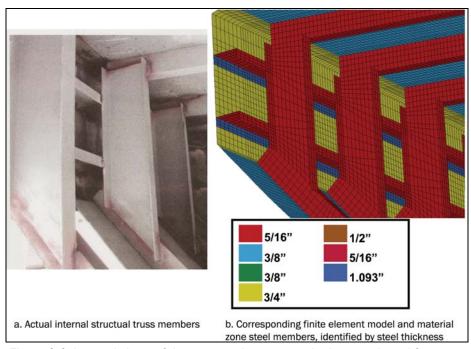


Figure 2.6. Internal views of the structural trusses at the bow as viewed from one side of the barge looking laterally across the barge.

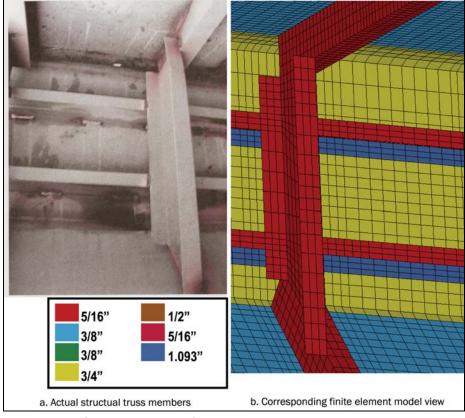


Figure 2.7. Another view of the interior showing the truss joining the C-channel of the bow.

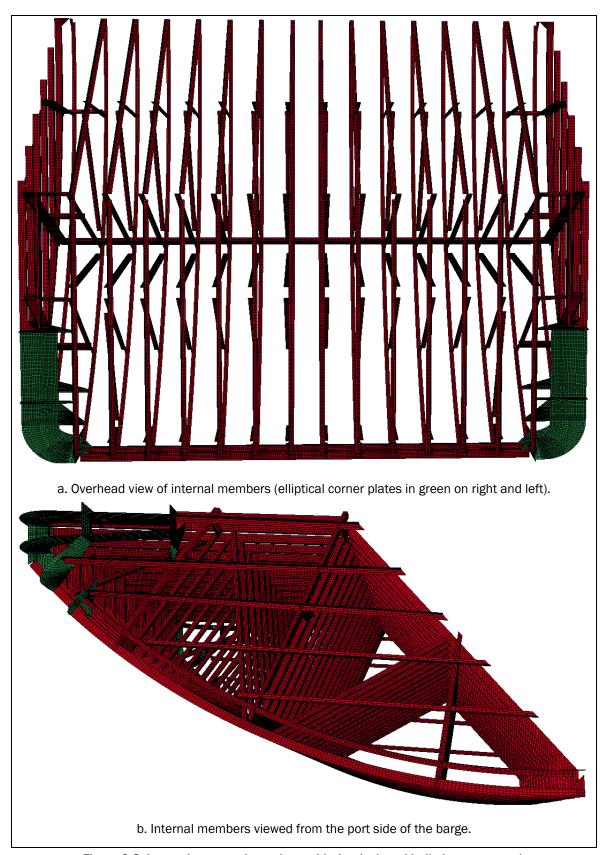


Figure 2.8. Internal structural members with the deck and hull plates removed.

2.3 Material modeling and material properties

With regard to material modeling used for the structural steel, significant yielding was expected to occur during crushing of the deck, hull plates, and the internal structural members in the headlog area of the bow along with the angle steel forming the truss members affected by the bow impact. As such, all shell elements in the model of the bow were specified with a plastic-multilinear material model matching the stress-strain data derived from tests conducted on plate steel obtained for an actual barge. A largedisplacement, large-strain formulation was used for the shell elements in the LS-DYNA impact analyses. Therefore, the true (Cauchy) stress and true (logarithmic) strain data were used (Figure 2.9). This material model for A-36 steel was obtained from tests conducted at the University of Florida on standard 18-in. tension coupon (Consolazio et al. 2002). The steel model for A-36 steel has an initial yield of 36 ksi $(2.48e + 08 \text{ N/m}^2)$, a yield strain of 0.0012, and a failure strain of 0.2. In the LS-DYNA analyses, the material model was specified as an effective stress versus effective plastic strain, LS-DYNA material number 24, *MAT_PIECEWISE_LINEAR_PLASTICITY. Other material model parameters specified as input are

- E = 30,000 ksi
- Poisson's ratio = 0.33
- Yield stress = 48 ksi
- Rupture stress = 86.6 ksi at 25 percent strain
- 20 percent plastic strain failure (i.e., effective plastic strain at failure (EPPF)).

Note that the rupture strain of 20 percent is specified in these LS-DYNA impact analyses. The implications are that when the strain reaches 20 percent, the strain integration point is removed from the analysis by LS-DYNA.

The LS-DYNA Material Model 24 allows for the addition of strain rate effects on the material using the Cowper-Symonds model. However, these simulations did not implement any strain rate effects for the A-36 steel material because the barge impact events are not high-speed impact simulations.

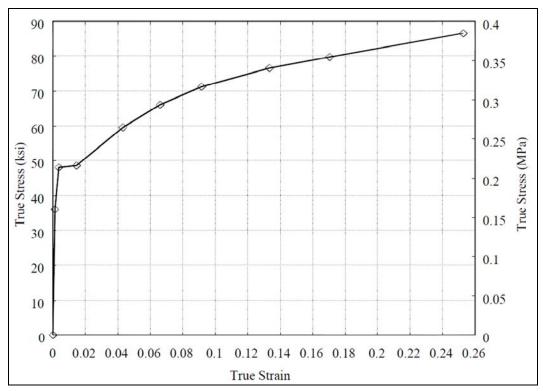


Figure 2.9. True stress versus true strain for A-36 structural steel (from Consolazio et al. 2002).

3 Limiting Impact Force Computations

3.1 Introduction

This chapter discusses the results of a series of 12 nonlinear finite element analyses using LS-DYNA and the 353,646-element mesh of the bow of a jumbo open-hopper barge with the assigned A-36 steel material properties discussed in Chapter 2. The object of the nonlinear finite element analysis was to compute the limiting impact force from yielding and buckling of the plates and internal structural framing at the bow of the barge during a head-on impact with a bullnose type structure such as those found at the end of a lock wall or with a concrete-filled cell structure. The nonlinear deformations were concentrated in the front half of the bow region. Impacts were made in such a manner that identical load conditions were evaluated for first contact occurring at two different bow locations. One location was the center of the bow (only plating material backed by transverse C-channel members exists at the center) as shown in Figure 3.1a. The second location was offset from the barge center line and in line with the first row of truss structures to the port side of center, 13.1875 in. from the center line of the barge as shown in Figure 3.1b.

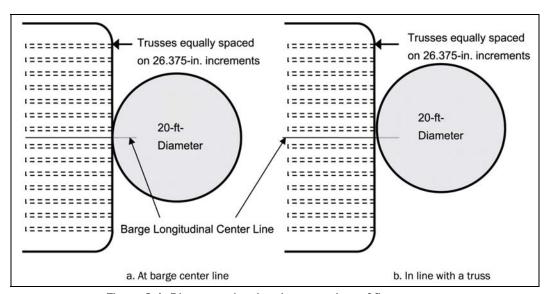


Figure 3.1. Diagrams showing the two points of first contact.

3.2 Nonlinear impact analyses

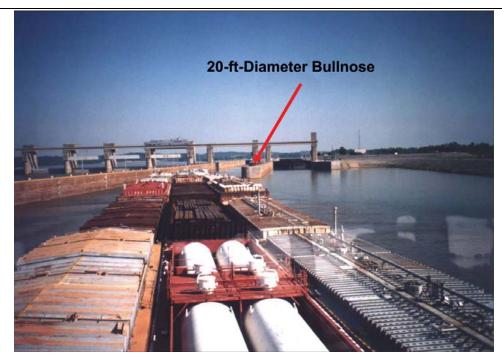
Lock approach walls are designed for usual, unusual, and extreme loads. Engineer Technical Letter (ETL) 1110-2-563 (Headquarters, U.S. Army Corps of Engineers (HQUSACE), 2004) provides a summary of the design requirements for these three load cases. The load cases are defined in terms of the annual probability of exceedance. The design information contained in HQUSACE (2004) is summarized in Table 3.1. This information also includes ranges for non-site-specific velocities (expressed in local barge coordinates) for the three load cases to use in preliminary analyses when site-specific traffic study results are not yet available.

The impacts that are the focus of this report are for head-on collisions. In a head-on impact the approach angle is 90 degrees, and the approach angle column in Table 3.1 is of no consequence for these analyses.

Table 3.1. Three design load condition categories, frequency of loadings, and typical ranges
for non-site-specific impact angles and approach velocities (from ETL 1110-2-563).

	Annual Probability of		Velocity, ft/sec		
Load Condition	Exceedance (Return Period)	Performance Criteria	Forward V _x	Lateral V _y	Approach Angle θ , deg
Usual	≥0.1 (1-10 years)	No damage	0.5-2.0	0.01-0.1	5-10
Unusual	<0.1 but >0.00333 (10-300 years)	Reparable damage	3.0-4.0	0.4-0.5	10-20
Extreme	<0.00333 (>300 years)	Noncollapse	4.0-6.0	<1.0	20-35

The concrete-filled cells and bullnose type structures chosen for these analyses have diameters of 20, 35, and 50 ft. The 20-ft diameter was chosen as one of the test parameters as this is the approximate diameter of the upstream bullnose between the two locks at Smithland Locks and Dam and is a typical bullnose size at rigid-wall lock and dams. A view of the upstream area of Smithland Lock and Dam showing the upstream middle wall bullnose is shown in Figure 3.2a. Figure 3.2b shows a close-up view of the bullnose.



a. Location of the bullnose between the two lock chambers.



b. Closer view of the bullnose, upper middle wall.

Figure 3.2. The upstream middle wall bullnoses at Smithland Locks and Dam.

The proposed flexible approach walls at Lock and Dams 22 and 25 consist of precast concrete beams supported by concrete-filled steel cells with a diameter of 35 ft. The cells at each end of the guide wall have a diameter of 50 ft. These dimensions are typical of flexible guard wall and guide wall designs. The cells at the ends of the guide walls are the cells that can be impacted by head-on collisions. Therefore 50-ft-diameter structures were chosen as another test parameter. Figure 3.3 presents the proposed wall design for Lock and Dam 22.

The authors felt that analysis of a third intermediate structure size would be beneficial. Analysis of more than two diameters could reveal relationships between forces and diameter sizes more readily than an analysis of only two diameters. A decision was made to include analysis of impacts with a 35-ft-diameter structure as well.

All impacts were made with the center barge impacting the bullnose headon in the analyses summarized in this report. That is, the direction of the
velocity vector was along the longitudinal line of the barge, which made
first contact with the most upstream point of the bullnose as shown in
Figure 3.4b or with the cell as shown in Figure 3.4a. For both of these
cases the velocity of the barge train normal to the structure was equal to V_x (using the Table 3.1 notation) and had no V_y component.

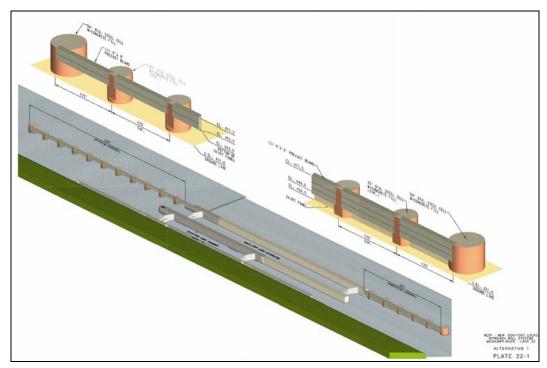


Figure 3.3. Proposed approach wall design for Lock and Dam 22.

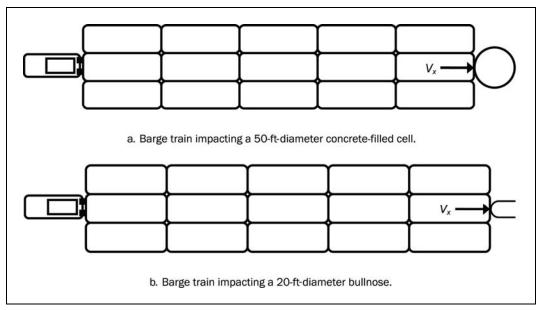


Figure 3.4. Barge train indicating movement in the x-direction only at impact.

Using the maximum forward velocities from Table 3.1 for the Usual and Extreme cases, the three diameters of the impacted structures and the two different impact locations (barge center line and in line with the truss), a combination of 12 sets of approach velocities, structure diameters, and impact locations were selected for analysis. Table 3.2 lists the structure diameters, approach velocities, and impact locations.

Diameter ft	Approach Velocity ft/sec	Impact Location
20	2	Center of Bow
35	6	Truss
50		

Table 3.2. Parameters that are the basis of the twelve test conditions.

3.3 Results

This section summarizes the computed results for the 12 nonlinear finite element analyses. The deck, the hull and internal plates, and the internal structural members all developed elastic and then plastic strains within the steel members as the rigid structure contacted the barge bow and then displaced the contact area of the bow.

Figure 1.1 shows the overhead views of the barge at initial contact with the structure and after 36 in. of penetration for Case 1. Case 1 is for the usual

velocity of 2 ft/sec impacting a 20-ft-diameter bullnose/cell. Impact location for Case 1 was at the bow center line between trusses. Figure 1.2 shows the force normal to the approach wall versus displacement of the bow's initial point of contact for this case. This force represents both the normal contact force applied to the approach wall and the force imparted by the wall onto the multi-degree-of-freedom structural system of the barge. The normal force ranges in value from 0 kip to a maximum force of 2400 kips at 9.6 in. of permanent normal deformation at the initial contact point. The LS-DYNA analysis of Case 1 continued until there was 36 in. of permanent deformation of the rigid wall into the impact area of the bow. The nonlinearity in Figure 1.2 results from (1) the nonlinear true-stress versus true-strain relationship for A-36 steel (Figure 2.9) and (2) the removal of strain integration points and elements when an effective plastic strain of 20 percent is achieved within the shell elements used to model the structural members and plates during the course of the crushing analysis of the bow.

Figure 3.5 shows the distribution of effective plastic strain at a permanent deformation of 9.6 in. at the point of impact with the bow for Case 1. Note the "crease" or standing wave of deformation in the deck plate in the upper right picture as well as the dimpling and creasing of the underside plates just below the vertical bow plate at this level of deformation. Figure 3.6 shows a close-up view of the distribution of effective plastic strain at the impact area (i.e., the bow center). Note the erosion (i.e., removal) of elements by LS-DYNA at the intersection of the vertical bow plate and the bottom plates; this results from an effective plastic strain of 0.2 (i.e., 20 percent) being achieved by shell elements within this zone. Figure 3.7 shows the distribution of von Mises stress at a permanent deformation of 9.6 in. at the point of impact for Case 1.

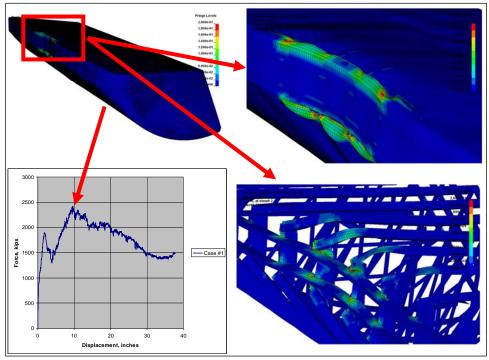


Figure 3.5. Distribution of effective plastic strain (in decimal fraction) at 9.6 in. permanent deformation and force versus displacement plot of the first contact point of the bow for Case 1, usual loading condition at the barge center line and impact with a 20-ft-diameter bullnose structure.

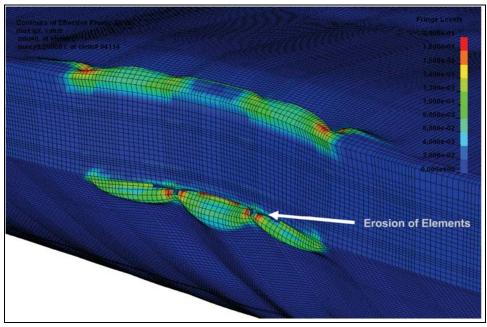


Figure 3.6. Distribution of effective plastic strain (in decimal fraction) at 9.6 in. of permanent deformation and erosion of elements in the impact area for Case 1, a usual loading condition impacting a 20-ft-diameter structure.

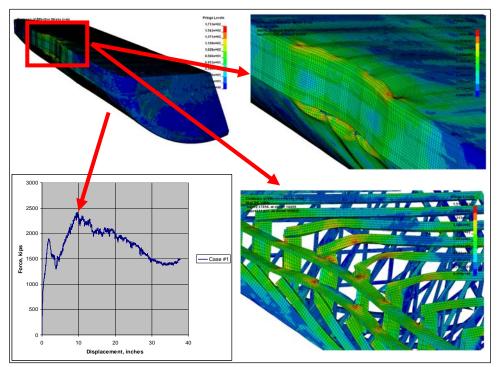


Figure 3.7. Distribution of von Mises stress at 9.6 in. permanent deformation and force versus displacement plot of the first contact point of the bow for Case 1, usual loading condition at the barge center line and impact with a 20-ft-diameter bullnose structure.

Figure 3.8 shows the distribution of effective plastic strain at a permanent deformation of 36 in. at the point of impact with the bow for Case 1. Note the multiple or standing waves of deformation and the large amount of bending in the deck plate in the upper right picture as well as the dimpling and creasing of the underside plates just below the vertical bow plate at this level of deformation. Figure 3.9 shows a close-up view of the distribution of effective plastic strain at the impact area (i.e., the bow center). Note the erosion (i.e., removal) of elements by LS-DYNA at the intersection of the vertical bow plate and the bottom plates as a result of an effective plastic strain of 0.2 (i.e., 20 percent) being achieved by shell elements within this zone. Figure 3.10 shows the distribution of von Mises stress at a permanent deformation of 36 in. at the point of impact for Case 1. Because of the nonlinear material response and the erosion of elements, the normal force at 36 in. of permanent deformation shown in Figure 1.2 is approximately 1,400 kips, a significant reduction from the maximum force of 2,400 kips at 9.6 in. of permanent normal deformation at the impact area at the center of the bow.

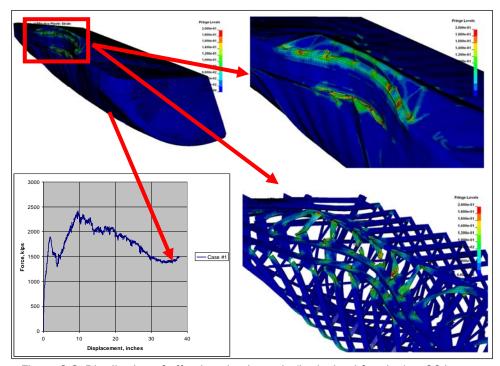


Figure 3.8. Distribution of effective plastic strain (in decimal fraction) at 36 in. permanent deformation and force versus displacement plot of the first contact point of the bow for Case 1, usual loading condition at the barge center line and impact with a 20-ft-diameter bullnose structure.

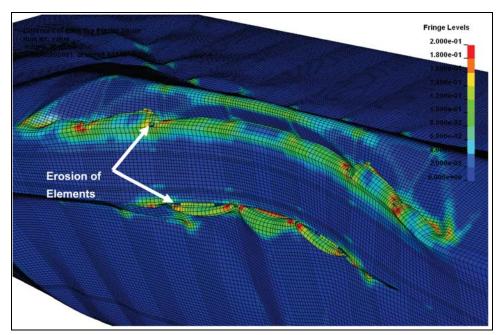


Figure 3.9. Distribution of effective plastic strain (in decimal fraction) at 36 in. of permanent deformation and erosion of elements in the impact area for Case 1, a usual loading condition impacting a 20-ft-diameter structure.

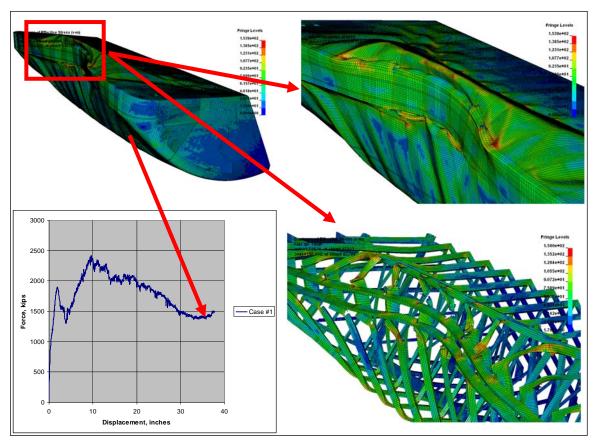


Figure 3.10. Distribution of von Mises stress at 36 in. permanent deformation and force versus displacement plot of the first contact point of the bow for Case 1, usual loading condition at the barge center line and impact with a 20-ft-diameter bullnose structure.

Figures 3.11-3.16 summarize the force normal to the wall versus displacement for the 12 LS-DYNA cases. The computations are made for 0-36 in. of permanent deformation normal to the structure at the point of initial contact. The 12 cases in Table 3.3 are presented in groups of two per figure. Odd-numbered LS-DYNA analysis cases correspond to impacts at 2 ft/sec while even-numbered LS-DYNA analysis cases correspond to impacts at 6 ft/sec. Each figure shares a common structure diameter (20, 35, or 50 ft) and initial impact location on the bow of the barge (center line or in line with a truss).

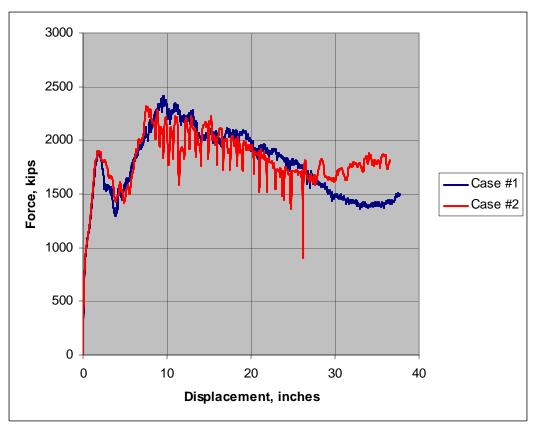


Figure 3.11. Force versus displacement curves for Cases 1 and 2.

The force versus displacement curves for Cases 1 and 2 are shown in Figure 3.11. Cases 1 and 2 are impacts with a 20-ft-diameter bullnose. Case 1 impacts at 2 ft/sec while Case 2 impacts at 6 ft/sec. For both cases there are two distinct peak values that are notable. For Case 1 a peak value of 1897 kips occurs at 1.90 in. of displacement. This is assumed due to the crushing of the vertical plating on the front of the headlog. After this resistance is encountered from the structural truss members, the force increases to a maximum force of 2414 kips at 9.65 in. of displacement. Case 2 displays an almost identical first peak of 1902 kips at 1.71 in. of displacement and a maximum value of 2316 kips at 7.54 in. of displacement.

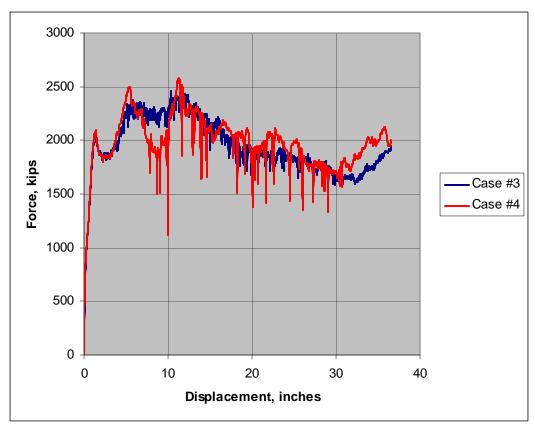


Figure 3.12. Force versus displacement curves for Cases 3 and 4.

Cases 3 and 4 are impacts with a 35-ft-diameter bullnose. Case 3 impacts at 2 ft/sec while Case 4 impacts at 6 ft/sec. The force versus displacement curves for these cases are shown in Figure 3.12. Cases 3 and 4 have very similar initial peak values of 2049 and 2096 kips at displacements of 1.37 and 1.41 in., respectively. The initial peak values are due to the crushing of the vertical headlog plates. As the structural truss members are crushed, the maximum force of 2483 kips for Case 3 is encountered at 11.62 in. of displacement. Likewise Case 4 shows a maximum force of 2577 kips at 11.27 in. of displacement caused by the crushing of the structural truss members.

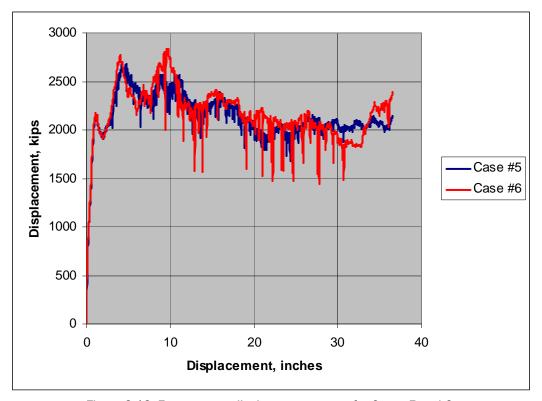


Figure 3.13. Force versus displacement curves for Cases 5 and 6.

The force versus displacement curves for Cases 5 and 6 are shown in Figure 3.13. Cases 5 and 6 are impacts with a 50-ft-diameter bullnose. Case 5 impacts at 2 ft/sec while Case 6 impacts at 6 ft/sec. For Case 5 the peak value of 2159 kips occurs at 1.18 in. of displacement. This is assumed due to the crushing of the vertical plating on the front of the headlog. After this resistance is encountered from the structural truss members, the force increases to a maximum force of 2682 kips at 4.80 in. of displacement. Case 6 displays an almost identical first peak of 2174 kips at 1.07 in. of displacement and a maximum value of 2836 kips at 9.58 in. of displacement.

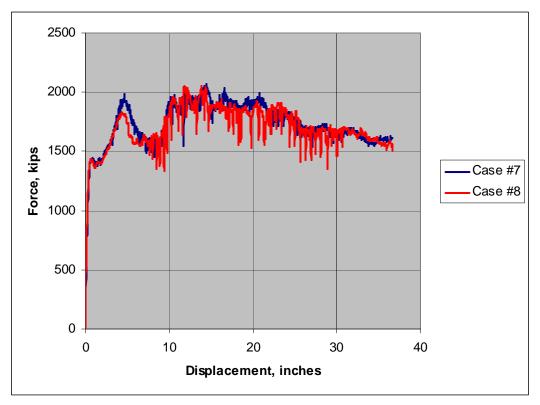


Figure 3.14. Force versus displacement curves for Cases 7 and 8.

Cases 7 and 8 are impacts with a 20-ft-diameter bullnose structure with the center of the impact occurring in line with a structural truss rather than at the center line of the barge as in Cases 1 through 6. The force versus displacement curves for Cases 7 and 8 are shown in Figure 3.14. These curves do not exhibit a decrease in force after the crushing of the headlog plates. The force continues to increase because of the crushing of the truss members in line with the impact until a peak force is achieved. For Case 7 the first peak force is 1984 kips at a displacement of 4.66 in. The maximum force due to further structural crushing is 2071 kips at 14.44 in. of displacement. For Case 8 the first peak force is 1836 kips at 4.31 in. of displacement. The maximum force from structural crushing is 2054 kips at 13.85 in. of displacement.

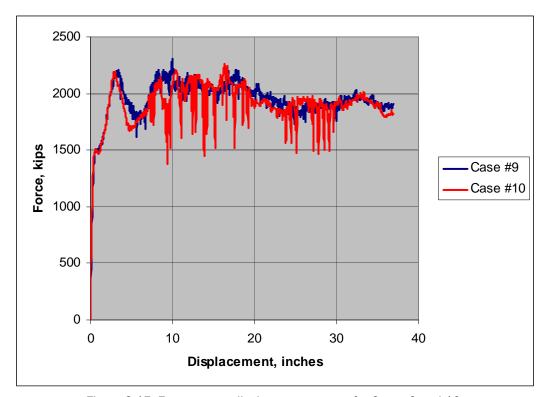


Figure 3.15. Force versus displacement curves for Cases 9 and 10.

Cases 9 and 10 impact with a 35-ft-diameter bullnose structure also in line with a truss of the barge. The force versus displacement curves for Cases 9 and 10 are shown in Figure 3.15. The crushing of the truss structure in line with the impact results in a first peak value for Case 9 of 2207 kips at 3.40 in. of displacement. Consequent crushing of the structural members yields a maximum force of 2308 kips at 9.98 in. of displacement for Case 9. Case 10 results indicate a first peak value of 2194 kips at 2.94 in. of displacement and a maximum force of 2265 kips at 16.35 in. of displacement.

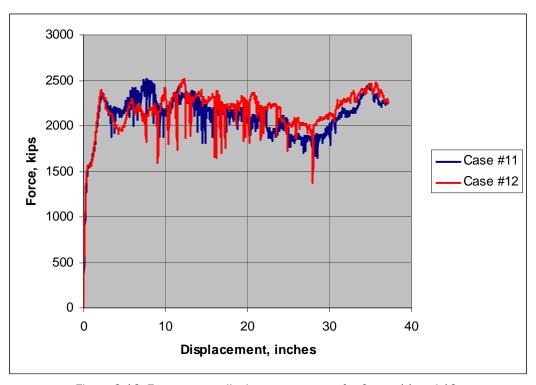


Figure 3.16. Force versus displacement curves for Cases 11 and 12.

Cases 11 and 12 impact with a 50-ft-diameter bullnose structure also in line with a truss of the barge. The force versus displacement curves for Cases 11 and 12 are shown in Figure 3.16. The crushing of the truss structure in line with the impact results in a first peak value for Case 11 of 2347 kips at 2.34 in. of displacement. Not much drop-off in forces occurs after this. The authors feel that this is due to the greater diameter bullnose structure engaging the additional structural truss members earlier than the smaller diameter structures. Consequent crushing of the structural members yields a maximum force of 2513 kips at 7.71 in. of displacement for Case 11. Case 12 results indicate a first peak value of 2399 kips at 2.20 in. of displacement and a maximum force of 2521 kips at 12.31 in. of displacement.

The maximum values indicated are summarized and shown in Table 3.3.

	Bullnose Diameter		Forward Velocity V _x		Initial Contact Location on	Maximum Force	Displacement at Maximum Force	First Peak Force	Displacement at First Peak Force
Case	in.	ft	in./sec	ft/sec	Bow	kips	in.	kips	in.
1	240	20	24	2	Center	2414	9.65	1897	1.90
2	240	20	72	6	Center	2316	7.54	1902	1.71
3	420	35	24	2	Center	2483	11.62	2049	1.37
4	420	35	72	6	Center	2577	11.27	2096	1.41
5	600	50	24	2	Center	2682	4.80	2159	1.18
6	600	50	72	6	Center	2836	9.58	2174	1.07
7	240	20	24	2	Truss	2071	14.44	1984	4.66
8	240	20	72	6	Truss	2054	13.85	1836	4.31
9	420	35	24	2	Truss	2308	9.98	2207	3.40
10	420	35	72	6	Truss	2265	16.35	2194	2.94
11	600	50	24	2	Truss	2513	7.71	2347	2.34
12	600	50	72	6	Truss	2521	12.31	2399	2.20

Table 3.3. Maximum values indicated during head-on barge impacts.

3.4 Comparison with an earlier finite element model

At the time these tests were performed, the authors decided to compare the results from one of the test conditions from a recently developed (2009) finite element model used to predict forces encountered by a jumbo hopper barge impacting bridge piers with results that could be obtained with the barge bow model described in this report. To that end, a test was conducted with the following parameters:

- 4-ft-diameter round impact structure
- 0.4 in./sec. impact velocity
- Impact at the center of the bow.

In the earlier Consolazio and Cowan (2003) nonlinear finite element analyses of a barge impacting a round (4-ft-diameter) rigid object at 0.4 in./sec., a peak force of about 715 kips was observed at 12 in. of deformation. The LS-DYNA analysis provided a peak force of 1290 kips at 5 in. of deformation (Figure 3.17). The authors consider this a significant difference. The Consolazio and Cowan work was performed using ADINA rather than LS-DYNA for the analyses. There are the obvious concerns regarding differences between the barge models caused by the size and layout of some of the structural angles and plates.

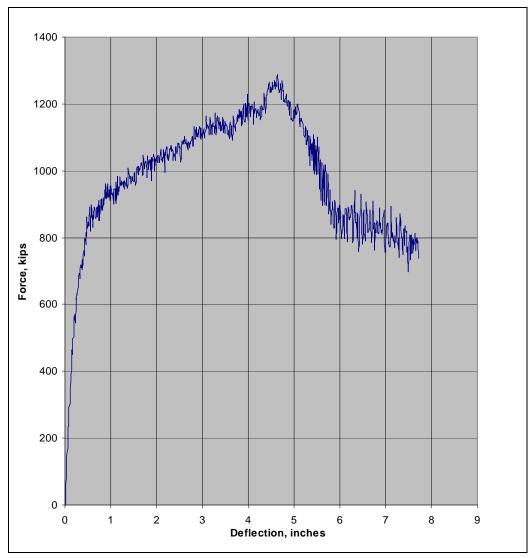


Figure 3.17. Force versus displacement curve for 4-ft-diameter impactor.

Also the finite element model presented in Chapter 2 of this report uses continuous joining of the fully integrated shell elements where parts (i.e., angles, plates, etc.) join together. Details on the finite element model were sparse in the 2003 Consolazio and Cowan paper. It was not known if the ADINA model joined parts in this manner or attempted to model spot welds, which may result in smaller impact forces, depending upon the impact angle and the orientation of the structural member. In reply to inquiries by the authors (e-mail message dated 10 February 2009) Dr. Gary Consolazio suspected that "the differences are most likely due to the resolution of the 2003 finite element model and to aspects of the dynamic stabilization procedures used in ADINA. …In our current generation of barge models, all members (angles, channels, etc.) are either fully discretized using shell elements or use beam elements with integrated

cross-sections and nonlinear material properties. In the ADINA model from 2003, portions of the finite element model utilized simpler resultant beam elements for efficiency. In addition, we now use only fully integrated shell elements in our models as you do." The most recent Consolazio head-on impact research results for his latest generation barge model are summarized in Consolazio et al. (2009) in which LS-DYNA is used to solve for the nonlinear force versus displacement of a single jumbo open hopper barge impact with a bridge support. By Equation 8 and by Figure 8.c in this Consolazio et al. (2009) paper, a peak force equal to 1125 kips was computed during an impact with a 4-ft-diameter (round) rigid structure. This is much more consistent with the LS-DYNA computed peak force result of 1290 kips in this report.

3.5 Comparison with AASHTO specification of impact force as a function of crush depth

In 1991, the American Association of State Highway and Transportation Officials (AASHTO) published a report that provided a guide specification for waterborne vessel collisions with highway bridges (AASHTO 1991). That report specified a means to compute depth of bow damage as a function of kinetic energy of the barge train (immediately prior to impact) and collision impact force as a function of the depth of bow damage. This approach assumes the kinetic energy translates directly to permanent bow deformation. That specification was taken from research conducted by Meir-Dornberg (1983). The AASHTO equation to compute bow damage is

$$a_{B} = \left[\left[1 + \frac{KE}{5672} \right]^{\frac{1}{2}} - 1 \right] \bullet \left[\frac{10.2}{R_{B}} \right]$$
 (3.1)

where:

 a_B = barge bow damage depth in feet

KE = barge impact energy in kip-feet

 R_B = ratio of $B_B / 35$

 B_B = barge width in feet.

The AASHTO specification further states the head-on collision force shall be determined in the following manner:

$$P_B = 4112 \bullet (a_B) \bullet (R_B)$$
 if $a_B < 0.34$ ft (3.2)

$$P_{B} = [1349 + 110 \bullet (a_{B})] \bullet (R_{B})$$
 if $a_{B} \ge 0.34$ ft (3.3)

where P_B is the static barge impact force in feet.

At a meeting of the U. S. Army Corps of Engineers Vessel/Barge Impact Product Delivery Team (PDT) ¹, committee members requested that the results of this research be compared with the AASHTO specification. This report section is dedicated to this task. It is important to remember for this discussion that the research effort discussed in this report is focused on quantifying the maximum force during an impact caused by the yielding of plates and headlog and the buckling of truss members within the bow region of the lead/impact barge. Neither the total mass of the barge (and its contents) nor the hydrodynamic effects of the water surrounding the barge are factors accounted for in this LS-DYNA analytical model. The AASHTO specification is a means to approximate the impact force and depth of damage to a barge based upon the kinetic energy of the barge during impact. As noted in Consolazio and Cowan (2003), the AASHTO specification computes the kinetic energy using Equation 3.4:

$$KE = \frac{C_H \bullet W \bullet (V)^2}{29.2} \tag{3.4}$$

where:

 C_H = hydrodynamic mass coefficient (factors the effect of the water surrounding the barge)

W = vessel weight in tonnes (1 tonne = 2205 lb)

V = impact velocity in ft/sec.

Since the entire impact barge, its mass, and its cargo represented in the finite element model are not available, the kinetic energy cannot be

¹ The meeting was conducted at the U.S. Army Engineer Research and Development Center, Information Technology Laboratory, in Vicksburg, MS, on March 11, 2009.

computed in the above manner. To rectify this, the potential energy for the barge in Case 1 of the subject LS-DYNA analysis was determined by computing the integral of the normal force as a function of the permanent barge displacement of the bow. This yielded the potential energy possessed by the crushing of the bow of the barge, shown in Figure 3.18. The normal force versus permanent deflection curve for Case 1 can be seen in Figure 3.11.

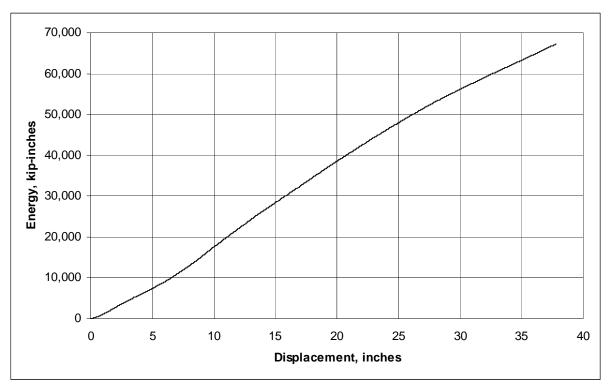


Figure 3.18. Barge bow potential energy for LS-DYNA analysis Case 1.

In actuality, during a head-on impact involving a moving barge of sufficient velocity (and KE) that the plates, headlog, and trusses within the bow region of the impacting front barge are crushed, the kinetic energy of the barge train immediately prior to impact is assumed for this simplified computation to be transformed into the barge bow's potential energy. Using this simplifying assumption, the energy values shown in the curve in Figure 3.18 from the LS-DYNA Case 1 analysis were set equal to the KE term used in Equation 3.1 to determine the equivalent AASHTO depth of damage for the impacting barge bow, damage depth a_B , for a head-on impact. Then the determined barge bow damage depth was used to compute the impact force P_B , according to the AASHTO specification using Equations 3.2 and 3.3. The AASHTO impact forces versus the AASHTO barge bow damage depth were plotted in Figure 3.19. The LS-DYNA

analysis Case 1 normal force versus displacement is also shown in Figure 3.19 for comparison.

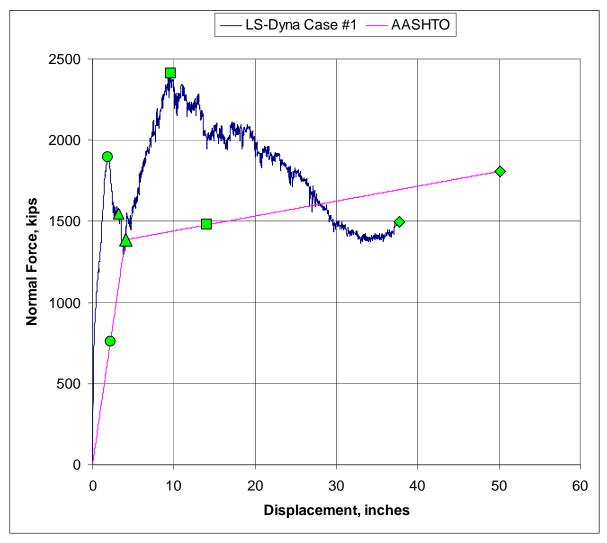


Figure 3.19. Force versus displacement curves for LS-DYNA analysis Case 1 and the corresponding AASHTO specification.

Four points from the two curves in Figure 3.19 are highlighted for comparison. The first point selected is the first peak force from the LS-DYNA Case 1 curve. The second point is at 4 in. displacement (0.34 ft) on the AASHTO curve (the point where the slope of the curve changes). The third point corresponds to the point of maximum force on the LS-DYNA curve. And the fourth point is the final point on the LS-DYNA Case 1 analysis curve, 37.76 in. The four selected points and their actual values are also reported in Table 3.4. The point number column refers to the particular sample from the two data sets.

		LS-DYN	A			AASHTO		
	Displacement		Normal Force	Potential Energy		ав		Рв
Point	in.	ft	kips	kip-in.	kip-ft	in.	ft	kips
51	1.9018	0.1585	1897.4	2478	206.5	2.208	0.184	756.8
85	3.2003	0.2667	1545.4	4641.6	386.8	4.104	0.342	1386.6
254	9.6501	0.8042	2413.8	16618.8	1384.9	14.1	1.177	1478.5
970	37.7589	3.1466	1494.6	67219.4	5601.6	50.2	4.180	1808.8

Table 3.4. Comparison of LS-DYNA and AASHTO specification results for the energy determined from LS-DYNA Case 1 analyses.

As can be observed by the study summarized using the four points listed in Table 3.4, for an equivalent amount of impact energy the AASHTO specification always results in a permanent deformation greater than that obtained by the LS-DYNA analyses. Also the LS-DYNA impact force for this case peaks before 10 in. of permanent deformation occurs. Because of the buckling and/or fracturing of the plates and internal structural members, a softening of the bow occurs and the impacting force decreases from the peak force. The LS-DYNA impact force becomes less than the AASHTO specification at about 28.5 in. of permanent deformation. This is in contrast to the AASHTO specification impact force that is a function of the crush depth and always increases as crush depth increases. Consolazio et al. (2009) also reported that peak impact forces occurred during their LS-DYNA analysis of barge impacts with bridge support structures before maximum crush depth was encountered.

3.6 Comparison with barges impacted using the 14-MN Statnamic load device

ETL 1110-2-563 (HQUSACE 2004) summarizes full-scale crushing experiments conducted in New Orleans, Louisiana, at the Halter Gulf Repair facilities during 21-23 June 2000. The experiments consisted of using two jumbo open-hopper 35- by 195-ft barges that were recently removed from service on the inland waterways and donated for the experiments. The barges were impacted using the 14-MN Statnamic load device owned by Applied Foundation Testing of Green Cove Springs, Florida. The Statnamic device is used primarily to test the axial and lateral capacities of piles and drilled shafts. The Statnamic device used for the experiments has the capability to deliver up to 2,400 kips of lateral force at a time duration similar to that of a barge impact. Figure 3.20 (Figure F-3

in ETL 1110-2-563) shows the Statnamic equipment and the experimental setup during the crushing experiments.



Figure 3.20. Statnamic device and experimental setup during experiment (Note: The detonation of the Statnamic device had just occurred at the time of the photograph) ((HQUSACE 2004)).

A total of nine experiments were conducted on both the barge corners and headlogs (front face of the barge above the rake) of the two barges to determine the impact forces and deformations of the components. The impact loads on the barges ranged from 400 kips up to 1,600 kips of lateral forces. Deformations range from no observable to a foot of displacement. Figure 3.21 (Figure F-4 in ETL 1110-2-563) shows the crushing damage to the headlog of the barge under an 800-kip force applied between rake trusses. Maximum deformation of the headlog in Figure 3.21 is approximately 9 in.



Figure 3.21. Crushing damage of barge headlog (from HQUSACE 2004).

Direct comparisons between the results of the field Statnamic impact experiments and the LS-DYNA analyses are not possible because deflections at the stages of loading by the Statnamic device were not made so as to develop figures similar to 3.11 through 3.17. However, some observations are made by the authors of this report:

- Table 3.3 peak force data and the peak force in Figure 3.17 show that the peak force encountered decreases with the diameter or equivalently, the width of the impactor.
- The Statnamic impactor with a width that is much smaller than that of a cellular structure and smaller than the 4-ft-diameter impactor discussed in Section 3.4 will yield smaller impact forces.
- For the Statnamic impactor, the peak forces encountered will vary dependent upon whether the impact occurs centered on a truss or between trusses. These locations were not reported in ETL 1110-2-563 (HQUSACE 2004).
- The lower force Statnamic tests that resulted in zero or nominal deformation likely did not contain a sufficient charge in the Statnamic

device to develop an impact force that can be associated with peak forces in the headlog during crushing. This would be analogous to determining the force on the "linear" portion of load versus deflection curve of Figures 3.11 through 3.16 for points that are below a point identified as 'first peak force" in Table 3.3.

- The 9 in. of crushing damage reported in ETL 1110-2-563 for Experiment 9 (Figure 3.21) may not be associated with the peak reported force of 800 kips.
- The deflection (and corresponding load) associated with the first peak force listed in Table 3.3 is likely dominated by the crushing of the headlog. As deflections increase, the truss system is engaged. This results in additional load-carrying capacity and a second peak force value, identified as Maximum Force in Table 3.3. Without deflection data (in the format of a load versus deflection curve) for the Statnamic impact tests, it is not possible to confidently determine with what stage of loading or level of structural system damage the reported force is associated.
- The barges tested were at the end of their service life. The LS-DYNA
 analyses were made using geometry and material properties of a new
 jumbo open-hopper barge. Therefore, higher impact forces are likely
 for the LS-DYNA analyses.

4 Summary, Results, and Conclusions

4.1 Summary

This research report discusses the results of a series of 12 nonlinear finite element analyses using LS-DYNA to compute the limiting impact force from the yielding and buckling of plates and internal structural framing at the impact point of the bow of a barge during its head-on impact with a bullnose structure at the end of a lock wall or with a concrete-filled cell structure. A finite element mesh of the bow of a jumbo open-hopper barge consisting of 357,897 nodes and 353,646 elements was constructed. Because of the localization of the nonlinear response during impact of the bow of the barge with the approach structure, only the bow region of the jumbo open-hopper barge (Figure 2.1) was modeled in the numerical analyses.

4.2 Results

Significant yielding occurred during crushing of the deck and hull plates and the internal structural members contained within the impact zone of the bow in all 12 analyses. All 12 numerical analyses were carried out until 36 in. of permanent deformation occurred at the first contact point of the bow of the barge. As such, all fully integrated shell elements in the model of the bow were specified with a plastic-multilinear material model matching the stress-strain data derived from tests conducted on A-36 plate steel obtained for an actual barge. A large-displacement, large-strain formulation was used for the shell elements in the LS-DYNA impact analyses and the true (Cauchy) stress, true (logarithmic) strain data (Figure 2.9) specified for this material model for the A-36 steel. These test results were obtained from tests conducted at the University of Florida on a standard 18-in. tension coupon tested by Anderson and summarized in Consolazio et al. (2002).

4.3 Conclusions

This technical report provides a basis for establishing the "capping force" when a barge train impacts a bullnose structure head-on. The capping force is based on the computation of the crushing force imparted during a head-on impact of the bow of a barge with a bullnose structure. When placed in a severe impact environment in which the bow begins to crush,

the bow acts like a structural fuseplug and provides for a limiting impact force applied to the approach structure by the barge train. The results of these 12 nonlinear finite element analyses of crushing of the barge bow definitively show a limiting force that may be transferred to a bullnose by the barge train through the front barge bow.

The magnitude of this limiting force ranges in value from 2050 to 2840 kips for the 12 analyses. The peak forces predicted were proportional to the diameter of the bullnose that was impacted as shown in Table 4.1. In all cases the peak force increased as the diameter of the bullnose increased. This was to be expected as more resistance from the plating and structural reinforcement is encountered because a larger cross section of the barge is engaged because of the larger bullnose diameter.

Cases 1-6 were identical to Cases 7-12 except for the point of first contact. Cases 1-6 made first contact at the center of the bow. Cases 7-12 made first contact in line with the truss just to the port side of the center line. In each instance the case that impacted at the center always resulted in a greater peak force than the corresponding case that made first impact at truss location (i.e., Case 1 yielded a larger peak force than Case 7, Case 2 was greater than Case 8, etc.).

Therefore, the peak force predicted is dependent upon the size of the bullnose impacted and the point along the bow where the impact occurs.

Table 4.1 Summary of maximum impact forces during head-on impacts.

	Maximum Forces Range, kips			
Diameter, ft	Minimum	Maximum		
20	2054	2414		
35	2265	2577		
50	2513	2836		

References

American Association of State Highway and Transportation Officials. 1991. *Guide Specification and Commentary for Vessel Collision Design of Highway Bridges, Volume I: Final Report.* Washington, DC.

- Consolazio, G. R., and D. R. Cowan. 2003. Nonlinear analysis of barge crush behavior and its relationship to impact resistant bridge design. *Computers and Structures* 81:547–557.
- Consolazio, G. R., R. A. Cook, and G. B. Lehr. 2002. *Barge impact testing of the St. George Island causeway bridge. Phase I: feasibility study.* Structures Research Report No. 783 to Florida Department of Transportation, UF Project No. 4504-783-12, Contract No. BC-354 RPWO #23. Gainesville, FL: Department of Civil and Coastal Engineering, College of Engineering, University of Florida.
- Consolazio, G. R., M. T. Davidson, and D. R. Cowan. 2009. Barge bow force-deformation relationships for barge-bridge collision analysis. *Transportation Research Board 88th Annual Meeting*, Washington, DC, January 11-15, 2009. Compendium of Papers DVD. Transportation Research Board: Washington, DC..
- Ebeling, R. M., and T. W. Warren. 2008. *Limiting impact force due to yielding and buckling of the plates and internal structural frame at the impact corner of the barge during its glancing blow impact with a lock approach wall.* ERDC/ITL TR-08-2. Vicksburg, MS: U.S. Army Engineer Research and Development Center.
- Headquarters, U.S. Army Corps of Engineers. 2004. *Barge impact analysis for rigid walls*. Engineer Technical Letter 1110-2-563. Washington, DC: Headquarters, U.S. Army Corps of Engineers.
- Livermore Software Technology Corporation. 2007. *LS-DYNA keyword user's manual, Version 971*. Vol 1. Livermore, CA: Livermore Software Technology Corporation.
- Meir-Dornberg, K. E. 1983. Ship collisions, safety zones, and loading assumptions for structures on inland waterways. VDI-Berichte 496:1-9.
- Rainsberger, R. 2006. *TrueGRID user's manual: a guide and a reference, Version 2.3.0.* Vols 1 and 2. Livermore, CA: XYZ Scientific Applications, Inc.

REPORT DOCUMENTATION PAGE

Form Approved OMB No. 0704-0188

Public reporting burden for this collection of information is estimated to average 1 hour per response, including the time for reviewing instructions, searching existing data sources, gathering and maintaining the data needed, and completing and reviewing this collection of information. Send comments regarding this burden estimate or any other aspect of this collection of information, including suggestions for reducing this burden to Department of Defense, Washington Headquarters Services, Directorate for Information Operations and Reports (0704-0188), 1215 Jefferson Davis Highway, Suite 1204, Arlington, VA 22202-4302. Respondents should be aware that notwithstanding any other provision of law, no person shall be subject to any penalty for failing to comply with a collection of information if it does not display a currently valid OMB control number. PLEASE DO NOT RETURN YOUR FORM TO THE ABOVE ADDRESS.

1. REPORT DATE (DD-MM-YYYY) August 2009	2. REPORT TYPE Final Report	3. DATES COVERED (From - To)
4. TITLE AND SUBTITLE	•	5a. CONTRACT NUMBER
Limiting Impact Force Due to Yield Frame at the Bow of a Barge during Structure	5b. GRANT NUMBER 5c. PROGRAM ELEMENT NUMBER	
6. AUTHOR(S)		5d. PROJECT NUMBER
Robert M. Ebeling and Terry W. W	arren	5e. TASK NUMBER
		5f. WORK UNIT NUMBER J4J37B
7. PERFORMING ORGANIZATION NAME	(S) AND ADDRESS(ES)	8. PERFORMING ORGANIZATION REPORT NUMBER
U.S. Army Engineer Research and Dev	velopment Center	
Information Technology Laboratory 3909 Halls Ferry Road		ERDC/ITL TR-09-3
Vicksburg, MS 39180-6199		
9. SPONSORING / MONITORING AGENC	Y NAME(S) AND ADDRESS(ES)	10. SPONSOR/MONITOR'S ACRONYM(S)
Headquarters, U.S. Army Corps of En	gineers	
Washington, DC 20314-1000		11. SPONSOR/MONITOR'S REPORT NUMBER(S)
12 DISTRIBUTION / AVAIL ARILITY STAT	CAMENT	

Approved for public release; distribution is unlimited.

13. SUPPLEMENTARY NOTES

14. ABSTRACT

This report presents a research study conducted to predict the impact forces that occur when a barge train impacts head-on with a circular concrete or concrete-filled structure. These structures are found at the end of lock approach walls as semicircles called bullnoses, as circular cells, and as mooring cells. This research was conducted using finite element analysis. A detailed finite element model of the bow of a jumbo hopper barge was created. LS-DYNA was used to perform impact simulations of the barge bow impacting differing diameters of cell structures and at varying approach velocities. In each case a "capping force" was found caused by the plating and internal structure acting as a "fuseplug" during the crushing of the bow.

Although research projects have been performed focused on corner barge impacts with lock walls, little research has been conducted in the area of forces from head-on collisions between a barge and a bullnose or a cell. A complementary R&D effort has been conducted by Dr. Gary Consolazio and his research associates at the University of Florida. His research has focused on a barge impacting a bridge pier. Comparison with their results has been made when it was appropriate.

15. SUBJECT TERMS

See reverse

16. SECURITY CLASS		17. LIMITATION OF ABSTRACT	18. NUMBER OF PAGES	19a. NAME OF RESPONSIBLE PERSON	
a. REPORT	b. ABSTRACT	c. THIS PAGE			19b. TELEPHONE NUMBER (include
UNCLASSIFIED	UNCLASSIFIED	UNCLASSIFIED		50	area code)

15. SUBJECT TERMS

Barge
Bullnose
Cellular structure
Crush analysis
Head-on
Impact
Limiting impact force for a barge train
Lock approach wall
LS-DYNA

Non-linear finite element analysis Plate buckling At the outset, many federal courts have observed that fraud claims often are not suitable for class treatment based on the varying degrees of the materiality of the fraud and the reliance on it by the proposed class members. See, e.g., Clark v. Prudential Ins. Co. of Am., 289 F.R.D. 144, 186-87 (D.N.J. 2013); see also Hurd v. Monsanto, 164 F.R.D. 234, 240 n.3 (S.D. Ind. 1995) ("Plaintiffs' fraud claims against both defendants are similarly inappropriate for class treatment. One necessary element in a fraud claim is reliance. Each class member will thus have to prove what acts or omissions of the defendants he actually relied upon and how that reliance caused his injury."); Perta v. Comprehensive Accounting Corp., No. 84-5484, 1985 WL 1900, at *3 (N.D. Ill. July 3, 1985) ("[T]he necessity of proving reliance by each class member upon the alleged fraudulent misrepresentations causes individual issues to predominate.").

Of course, there are exceptions to the rule. But Plaintiffs do not engage at all with the nuances of the multiple regimes of state common-law they invoke. Instead, they conclusorily assert that, "because they require no individual inquiries into particular consumers' reliance or decision-making processes," the claims can be certified. ECF No. 38, PageID.2156. Their support for this sweeping conclusion lies buried in a footnote which contains a string of unexplained citations. *Id.* at PageID.2155 n.8.

The Court has reviewed the cases cited in this footnote and is not persuaded that they are germane to the issue. And from its independent

research of the state law governing these claims, it is not persuaded that reliance can be presumed so broadly in each instance.⁵ The Court also has additional concerns, which Plaintiffs have not even begun to address. Do these state common-law claims require privity? How can Plaintiffs show, with common proof on a class-wide basis, that *New* GM

⁵ See, e.g., Univ. Fed. Credit Union v. Grayson, 878 So.2d 280, 287 (Ala. 2003) (observing that "fraud actions are not often well suited for classaction certification" because they "involve numerous misrepresentations and varying kinds of degrees of reliance, all of which create individualized issues"); Schock v. Jacka, 460 P.2d. 185, 188 (Ariz. 1969) ("The gist of an action based on fraud is fraud in defendant and damage to plaintiff; and its basic elements are false representations by defendant and reliance thereon by plaintiff to his damage."); GCA Strategic Inv. Fund v. Joseph Charles & Ass., Inc., 537 S.E.2d 677, 681-82 (Ga. Ct. App. 2000) (observing that "[t]he essential elements to an action in tort for damages resulting from a material misrepresentation constituting fraud are: (1) that the defendant made the representations; (2) that at the time he knew they were false ...; (3) that he made them with the intention and purpose of deceiving the plaintiff; (3) that the plaintiff [justifiably] relied on such representations; [and] (5) that the plaintiff sustained the alleged loss and damage as the proximate result of their having been made"): Wells v. Stone City Bank, 691 N.E.2d 1246, 1250 (Ind. Ct. App. 1998) (holding that a party generally must prove five elements: 1) that there was a material misrepresentation of past or existing fact; 2) that the representation was false; 3) that the representation was made with knowledge or reckless ignorance of its falsity; 4) that the complaining party relied on the representation; and 5) that the representation proximately caused the complaining party's injury); *Philip Morris Inc. v.* Angeletti, 752 A.2d 200, 234 (Md. App. 2000) ("Success in Maryland on a civil claim of fraud requires proof of reliance".); Hord v. Envtl. Research Inst. of Mich., 617 N.W.2d 543, 550 (Mich. 2000) ("A legal duty to make a disclosure will arise most commonly in a situation where inquiries are made by the plaintiff, to which the defendant makes incomplete replies that are truthful in themselves but omit material information.").

fraudulently concealed information from class members who purchased used vehicles, manufactured by *Old* GM, from *private* entities? Can this proof be the same as for class members who purchased New GM vehicles from GM-authorized dealerships? Plaintiffs' lack of engagement with the substantive state law precludes certification. It was their burden affirmatively demonstrate that common issues susceptible to class-wide proof will predominate.

4. Damages Model

GM also attacks Plaintiffs' damages model as inconsistent with their theory of liability. Under *Comcast Corp v. Behrend*, 569 U.S. 27, 35 (2013), Plaintiffs must present a damages model adequately tethered to their theory of liability to satisfy Rule 23. "Calculations need not be exact, but at the class-certification stage (as at trial), any model supporting a plaintiff's damages case must be consistent with its liability case." *Id.* (internal quotations and citations omitted).

Plaintiffs now say they are seeking only overpayment damages and that they will be able to present an overpayment model. But their only evidence of a model comes from a declaration by their expert, Edward Stockton. Though Stockton says what he will produce at some point in the future is an "overpayment" model, he appears to be calculating repair costs. Stockton acknowledges that some class members may have received repairs, that some class members may no longer own their vehicles, and that the usefulness of a vehicle diminishes over time. In lieu

of actually demonstrating how he would incorporate variables, however, he asserts only conclusorily that he will be able to factor them in at some point in the future. He does not acknowledge in his declaration the considerable issues posed by GM's bankruptcy and the split in liabilities.

The Court is not persuaded that, at this stage, this showing is enough or that Stockton's descriptions of the model he intends to create are sufficient. As explained above, Plaintiffs' ability to demonstrate damages is considerably hampered by several different factors.

E. Superiority

Although the Court has already identified numerous barriers to the certification of class, it will briefly address superiority. Factors relevant to this inquiry include "the class members' interests in individually controlling the prosecution or defense of separate actions" and "the likely difficulties in managing a class action." Fed. R. Civ. P. 23(b)(3).

The Court finds that class action treatment is neither superior nor manageable in this case. While the likely need for expert testimony to establish the existence of the defects alleged may inhibit certain putative class members from pursuing individual actions, the tidal wave of individual issues will swamp the litigation. The proposed classes—which include new and used vehicles manufactured over the course of seven years by two different entities, purchased under a variety of different circumstances during a nearly two-decade-long period—are sprawling, unwieldy, and raise a variety of unique defenses to GM.

Additionally, the fact that Plaintiffs also wish to pursue claims

under the laws of twenty different states which they have demonstrated

no familiarity with makes class treatment of the case unmanageable. The

Sixth Circuit has recognized that, in multi-state class actions, variations

in state law may overwhelm common issues and impose upon this Court

the "impossible task of instructing a jury on the relevant law." *Pilgrim v*.

Univ. Health Card, LLC, 660 F.3d 943, 948 (6th Cir. 2011) (internal

quotations omitted).

V. CONCLUSION

Plaintiffs have failed to carry their burden to establish that

certification of any of the proposed classes is appropriate. Accordingly,

for the reasons set forth above, IT IS ORDERED that Plaintiff's motion

for class certification is **DENIED**.

IT IS FURTHER ORDERED that, within 30 days of this Opinion

& Order, counsel shall meet and confer about how to proceed with the

individual claims asserted in this action by the Named Plaintiffs. An

order setting a status conference to discuss scheduling shall follow.

IT IS SO ORDERED, this 30th day of September, 2023.

BY THE COURT:

/s/Terrence G. Berg

TERRENCE G. BERG

United States District Judge

56